Available online at www.sciencedirect.com

ScienceDirect

Ceramics International 35 (2009) 1045–1049

CERAMICS INTERNATIONAL

www.elsevier.com/locate/ceramint

Preparation of spinel ferrites from citrate precursor route—A comparative study

B.S. Randhawa*, H.S. Dosanjh, Manpreet Kaur

Department of Chemistry, Guru Nanak Dev University, Amritsar 143005, India

Received 4 March 2008; received in revised form 19 March 2008; accepted 22 April 2008

Abstract

Spinel ferrites MFe_2O_4 (M = Mn, Co, Ni, Cu) have been prepared from the thermolysis of transition metal bis(citrato)ferrates(III), $M_3[Fe(C_6H_5O_7)_2]_2 \cdot xH_2O$. Various physico-chemical studies, i.e. TG–DTG–DSC, XRD and Mössbauer spectroscopy have been employed for the investigation of the mode of decomposition and characterization of intermediates/products formed. After dehydration the anhydrous precursor undergoes an oxidative decomposition to yield α-Fe_2O_3 and respective metal oxide. Finally spinel ferrites, MFe_2O_4, are formed as a result of a solid-state reaction between the oxides at a much lower temperature (310–440 °C) and in less time as compared to that of the conventional ceramic method. SEM studies show these ferrites to be of nanosized. Ferrites obtained from the thermolysis of transition metal ferricitrate precursors show higher values of saturation magnetization than those got from respective ferrimalonate precursors, thus designating the former as novel materials to operate at high frequencies.

Keywords: A. Calcination; B. X-ray method; D. Ferrites; Mössbauer spectroscopy

1. Introduction

Spinel ferrites have received renewed interest in technologically anchored modern society due to their promising magnetic properties [1,2]. They find an extensive application in microwave devices, radar, digital recording, ferro-fluids, catalysis and magnetic refrigeration systems [3–5]. Preparation of ferrites by the conventional ceramic method has many disadvantages, viz. non-homogeneity, large particle size and low surface area. Precursor method, on the other hand, has become a fascinating subject of recent interest because of better micro-structural and compositional control achievable. Owing to their complexing ability, sensitivity towards oxidation state and ease of decomposition, metal ferricarboxylates have proven to be the most suitable precursors for the preparation of ferrites. Although thermolysis of transition metal ferrioxalates/maleates [6,7] has been investigated in detail, a similar interest on respective ferricitrates needs to be generated.

2. Experimental procedure

The metal ferricitrate precursors, $M_3[Fe(C_6H_5O_7)_2]_2 \cdot xH_2O$ (M = Mn, Co, Ni, Cu) were prepared by mixing stoichiometric quantities of aqueous solutions of ferric citrate, citric acid and respective metal nitrate. The reaction mixture was refluxed at 100 °C for 10 h and then concentrated on water bath. The fluffy concentrated precursor, thus obtained, was kept in an oven at 60 °C for 2 h. The resultant precursor powder obtained was then washed with ethanol, dried and stored in vacuum desiccator. The identity of the precursors was established by elemental analysis. The experimental details of various techniques employed are reported elsewhere [8].

3. Results and discussion

Room temperature Mössbauer spectra of the precursors exhibit a doublet (as an example Fig. 1 shows the spectrum of manganese precursor) with isomer shift (δ) and quadrupole splitting (Δ) values in the ranges 0.36–0.39 mm s^{-1} and 0.57–0.59 mm s^{-1}, respectively. These parameters agree with those reported for the high spin Fe(III) complexes with octahedral geometry [9].

---

* Corresponding author.
E-mail addresses: balwinderrandhawa@yahoo.co.in (B.S. Randhawa), chemi_dosanjh@yahoo.com (H.S. Dosanjh).

0272-8842/$34.00 © 2008 Elsevier Ltd and Techna Group S.r.l. All rights reserved.
doi:10.1016/j.ceramint.2008.04.031

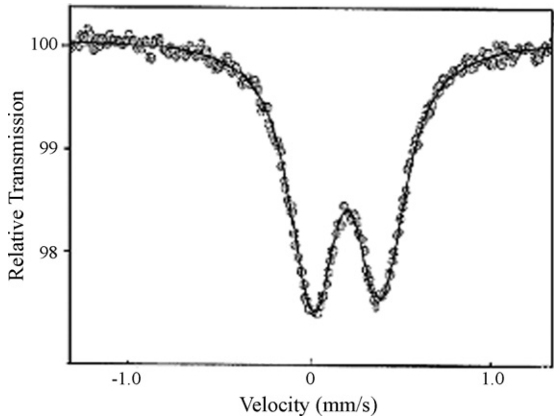

Fig. 1. Room temperature Mössbauer spectrum of manganese bis(citrato)ferrate(III) octahydrate.

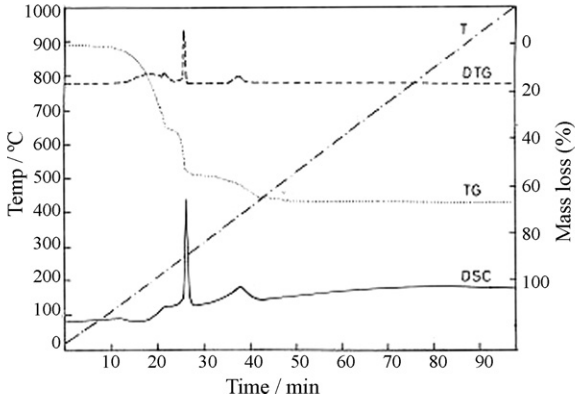

Fig. 2. Simultaneous TG–DTG–DSC curves of manganese bis(citrato)ferrate(III) octahydrate.

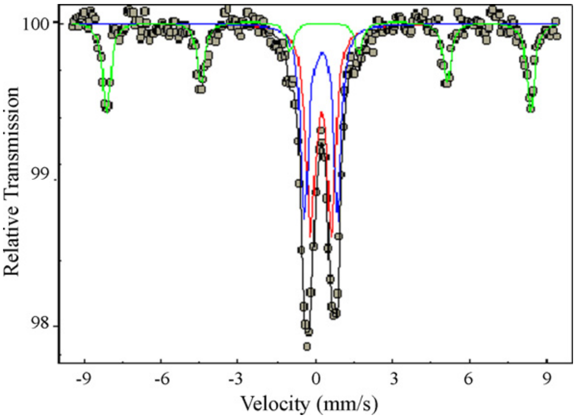

Fig. 4. Mössbauer spectrum of the final residue.

Fig. 2 displays the simultaneous thermal analysis (STA), i.e. TG–DTG–DSC curves of manganese bis(citrato)ferrate(III) octahydrate at a heating rate of 10 °C min^{-1}. Dehydration and decomposition of the complex occur simultaneously until a mass loss of 36% is reached at 250 °C marking the presence of manganese acetone-dicarboxylate, $MnC_5H_4O_5$ and Fe_2O_3. These thermal changes are clearly reflected by a DSC peak which initially started as endotherm (due to dehydration, ΔH = 294.3 kJ mol^{-1}) but subsequently became exotherm at higher temperature (due to decomposition, $\Delta H = -175.4$ kJ mol^{-1}). There exist two respective peaks in DTG also. The presence of Fe_2O_3 has been confirmed by Mössbauer spectrum (Fig. 3) of the residue, obtained by isothermal calcination of the precursor at 250 °C for 15 min, which shows a doublet having parameters comparable to those reported for α-Fe_2O_3 with particle size <10 nm.

As heating continues, manganese acetone-dicarboxylate undergoes a rapid oxidative decomposition to MnO. The corresponding mass loss of 57% at 280 °C indicates that only two moles of acetone-dicarboxylate have decomposed. There are strong peaks in DSC (exo, $\Delta H = -1235.8$ kJ mol^{-1}) and DTG at 275 and 270 °C, respectively. At higher temperature there is a gradual decomposition of the remaining one mole of acetone-dicarboxylate followed by a solid-state reaction between MnO and Fe_2O_3 leading to the formation of manganese ferrite, $MnFe_2O_4$. This step involving oxidative decomposition (supported by a DTG peak) and a subsequent solid-state reaction is accompanied by a broad exotherm centered at 395 °C. A high

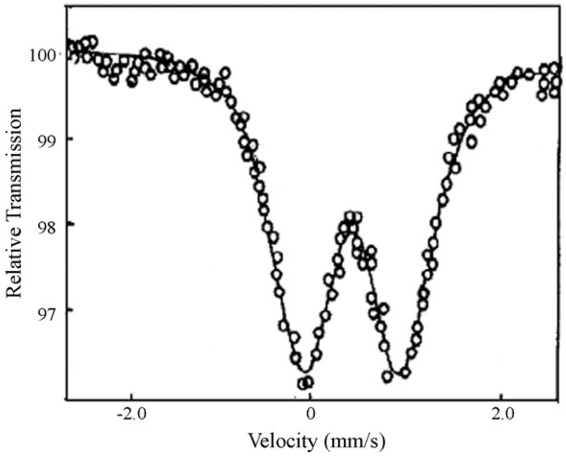

Fig. 3. Mössbauer spectrum of the residue obtained by calcining manganese ferricitrate at 250 °C for 15 min.

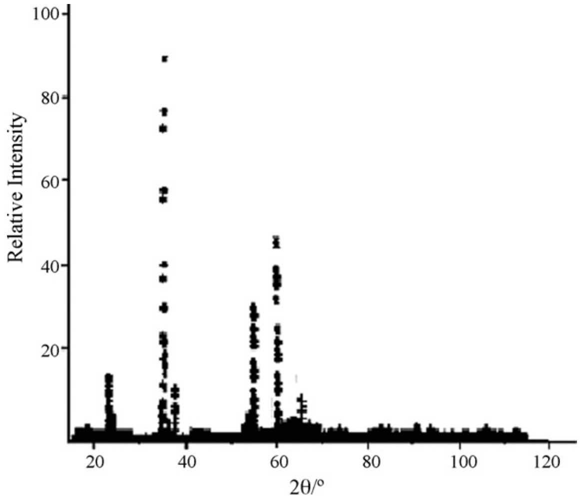

Fig. 5. XRD powder pattern of the final thermolysis residue after calcining at 500 °C for 3 h. .

Table 1
Mössbauer parameters of the thermolysis products of $M_3[Fe(C_6H_5O_7)_2]_2 \cdot xH_2O$ at 77 K

M	Calcining temperature (°C)	δ (mms^{-1})	Δ (mms^{-1})	B^* (T)	%Fe^{3+} distribution	Assignment
Mn	250	0.34	0.87	(CD)	–	α-Fe_2O_3
	400	0.47	0.68	(CD)	26	$MnFe_2O_4$
		0.48	1.61	(CD)	42	
		0.49	–	53.5(S)	32	
Co	300	0.47	0.07	53.5(S)	20	α-Fe_2O_3
		0.36	0.02	50.3(S)	50 (o)	$CoFe_2O_4$
		0.40	–	47.0(S)	30 (t)	
	350	0.48	0.01	53.4(S)	48 (o)	$CoFe_2O_4$
		0.39	–	50.8(S)	52 (t)	
Ni	300	0.47	–	54.3(S)	18	α-Fe_2O_3
		0.39	–	50.1(S)	46 (o)	$NiFe_2O_4$
		0.43	–	44.3(S)	36 (t)	
	350	0.46	0.03	55.6(S)	46 (o)	$NiFe_2O_4$
		0.35	–	51.2(S)	54 (t)	
Cu	350	0.48	–	54.2(S)	46 (o)	$CuFe_2O_4$
		0.36	–	50.8(S)	54 (t)	

#w.r.t. pure iron absorber, B^* = internal magnetic field in tesla (T), S = sextet, CD = central doublet, o = octahedral, t = tetrahedral.

value of ΔH (-1157 kJ mol^{-1}) for the exotherm clearly demonstrates the vigorousness of the oxidative pyrolysis, which is a characteristic feature of carbonaceous citrate ligands during thermolysis. Mössbauer spectrum of the final thermolysis residue (at 77 K) (Fig. 4) exhibits a six-line pattern along with a central doublet due to co-existence of ferrimagnetic and superparamagnetic domains of the ultrafine ferrite ($MnFe_2O_4$) particles. The central doublet has been resolved into two sites (octahedral and tetrahedral) having isomer shift and quadruple splitting values of 0.48 and 0.47 mm s^{-1} and 1.21 and 0.68 mm s^{-1}, respectively. The sextet shows an isomer shift and internal magnetic field (B) values of 0.49 mm s^{-1} and 53.5 T, respectively. The Mössbauer parameters listed in Table 1 agree with those reported for manganese ferrite [6]. XRD powder pattern (Fig. 5) of the final thermolysis residue also shows the presence of manganese ferrite. SEM micrograph (Fig. 6) reveals the presence of ferrite with average particle size of 30 nm.

Fig. 7 displays the simultaneous (TG–DTG–DSC) thermograms of cobalt bis(citrato)ferrate(III) decahydrate at a heating rate of 10 °C min^{-1}. The dehydration of the complex takes place in two steps, in the first installment a mass loss of 6.7% up to 127 °C indicates the removal of five water molecules. DSC displays a crescent shaped endotherm centered at 100 °C ($\Delta H = 244.6$ kJ mol^{-1}), while the respective DTG peak lies at 105 °C. A further rapid change in mass loss up to 31.8% suggesting the removal of rest of five lattice water molecules is immediately followed by the decomposition of the anhydrous complex into cobalt acetone-dicarboxylate and Fe_2O_3. These thermal changes are accompanied by a DTG peak at 140 °C which is exo in DSC with $\Delta H = -239.7$ kJ mol^{-1}. The intermediate (acetone-dicarboxylate) does not show any stable arrest in TG and continues to decompose gradually till a mass loss of 48% is reached at 240 °C suggesting the decomposition of one mole of cobalt acetone-dicarboxylate into CoO. The corresponding sharp exotherm ($\Delta H = -607.8$ kJ mol^{-1}) and DTG peak lie at 215 °C. As heating continues, the remaining two moles of acetone-dicarboxylate decompose to oxide phase as shown by a steep mass loss of 68.6% at 300 °C. The

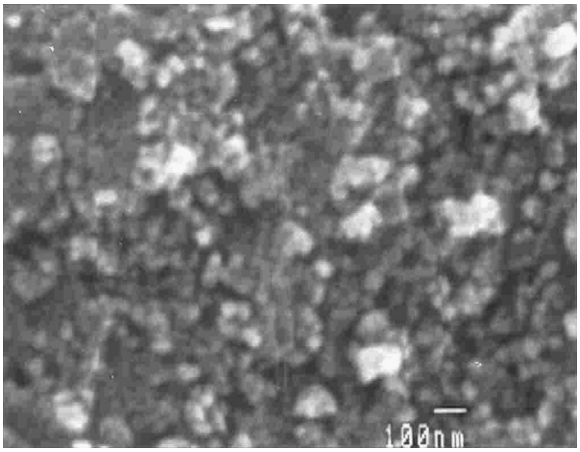

Fig. 6. SEM micrograph of the final residue.

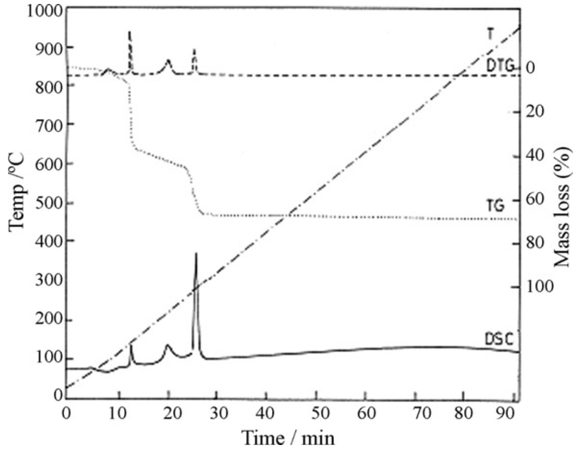

Fig. 7. Simultaneous TG–DTG–DSC curves of cobalt bis(citrato)ferrate(III) decahydrate.

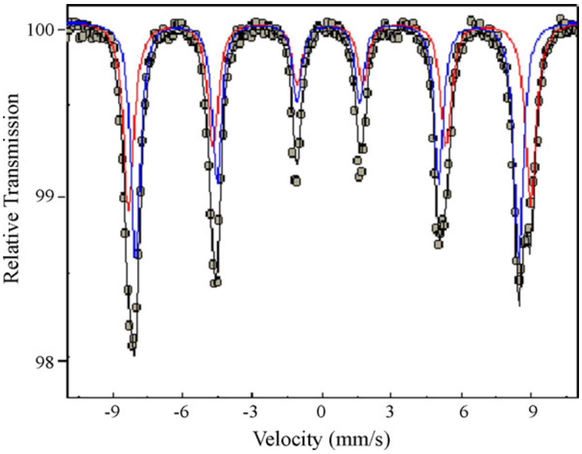

Fig. 8. Mössbauer spectrum of the final residue.

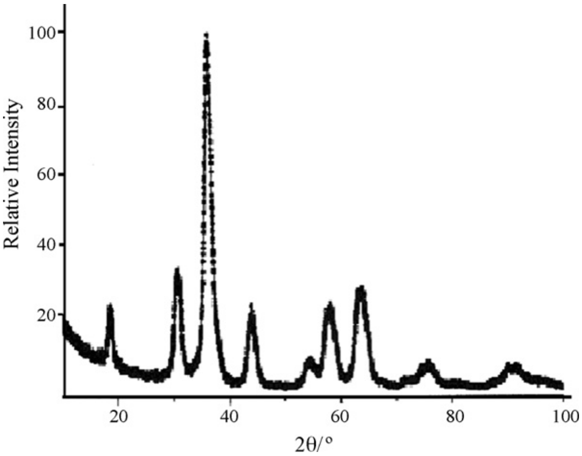

Fig. 9. XRD powder pattern of the final residue.

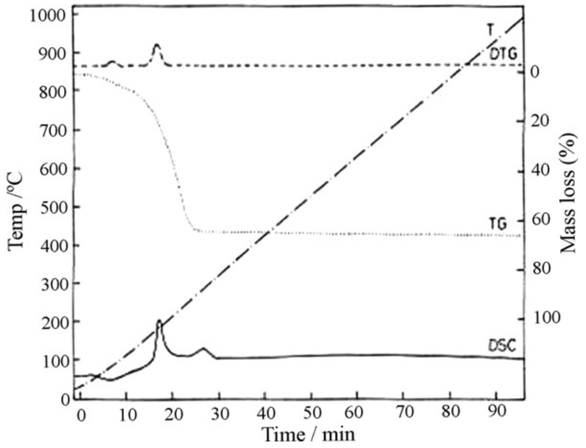

Fig. 10. Simultaneous TG–DTG–DSC curves of copper bis(citrato)ferrate(III) hexahydrate.

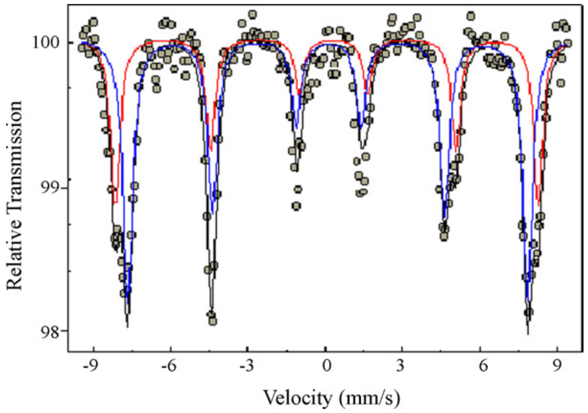

Fig. 11. Mössbauer spectra of the final thermolysis product.

respective DTG and DSC (exo, $\Delta H = -2076.5$ kJ mol^{-1}) peaks lie at 280 °C. Mössbauer spectrum of the residue obtained by calcining the parent complex at 300 °C for 15 min displays three overlapping sextets (at 77 K), the parameters for which reveal the presence of Fe_2O_3 and $CoFe_2O_4$. As heating continues the solid-state reaction between Fe_2O_3 and CoO completes and leads to the formation of pure $CoFe_2O_4$.

Mössbauer spectrum (Fig. 8) of the final thermolysis residue (at 77 K) displays two overlapping sextets, the parameters for which confirm the existence of $CoFe_2O_4$. The identity of cobalt ferrite has also been confirmed by XRD powder pattern (Fig. 9) of the final thermolysis residue.

Nickel ferricarboxylate precursor has been found to follow almost similar pattern of thermal decomposition, finally leading to the formation of $NiFe_2O_4$.

The simultaneous TG–DTG–DSC curves of copper bis(citrato)ferrate(III) hexahydrate are displayed in Fig. 10. From these curves it is clearly evident that the thermolysis occurs in two major steps, i.e. dehydration and subsequent decomposition of the anhydrous complex into oxide phase. A similar decomposition scheme has also been reported for copper ferrioxalate [6]. The dehydration completes at 140 °C with a mass loss of 9.0% (calc. loss = 9.3%). DTG and DSC (endo, $\Delta H = 233.3$ kJ mol^{-1}) show weak broad signals centered at 100 °C suggesting a slow rate of dehydration. The anhydrous complex is not stable and undergoes a rapid mass loss up to 66% at 260 °C. This mass loss indicates the formation of Fe_2O_3 and CuO (calc. loss = 65.8%), the identities of which have been confirmed by the XRD powder pattern of the residue obtained by calcining the parent complex isothermally at 260 °C for 15 min. The corresponding DTG and DSC (exo, $\Delta H = -2683$

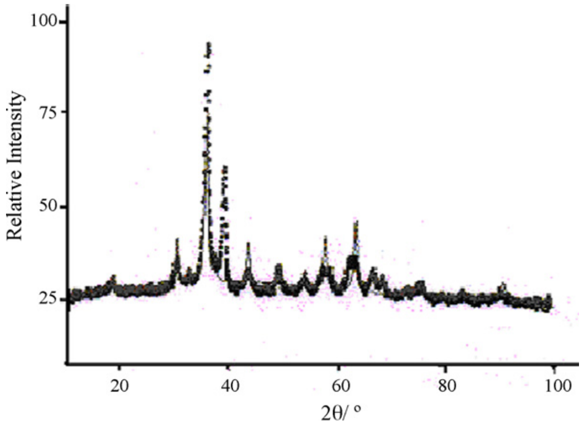

Fig. 12. XRD powder pattern of the final thermolysis residue.

Table 2
Magnetic parameters of the ferrites obtained

MFe_2O_4	Density (g/cm^3)	Saturation magnetization (Gauss)	Gauss (cm^3)	T_c (°C)	Average particle size (nm)
$MnFe_2O_4$	4.62	2546	551	305	30
$CoFe_2O_4$	5.31	3223	607	513	35
$NiFe_2O_4$	5.36	3002	560	582	35
$CuFe_2O_4$	5.42	2835	523	450	40

kJ mol^{-1}) peaks lie at 185 and 190 °C, respectively. The presence of another exotherm ($\Delta H = -337$ kJ mol^{-1}) at higher temperature (297 °C) suggests a solid-state reaction between the oxides to yield pure copper ferrite, $CuFe_2O_4$. The existence of copper ferrite has been confirmed by Mössbauer spectrum (Fig. 11) of the final thermolysis residue, which displays two overlapping sextets, the parameters of which (Table 1) correspond to those reported for copper ferrite [10]. XRD powder pattern of the final thermolysis product (Fig. 12) confirmed the existence of copper ferrite, $CuFe_2O_4$. SEM analysis reveals the formation of ferrite particles with an average particle size of 40 nm.

4. Magnetic properties

The ferrite nanoparticles prepared by citrate precursor route have shown promising values of magnetic parameters (Table 2), exploring their potentiality to operate at high/microwave frequencies.

5. Conclusion

The temperature range for ferrite formation (310–440 °C) is lower than that of the respective oxalate/malonate and maleate precursors. This is attributed to the fact that the carbonaceous citrate precursor, upon thermolysis, liberates an enormous amount of heat (clearly visible from ΔH values) that autocatalyses further decomposition process, thus lowering the external temperature required for ferrite formation.

References

[1] M.R. DeGuire, G. Kalonji, R.C. O'Handley, Cation distributions in rapidly solidified cobalt ferrite, J. Am. Ceram. Soc. 73 (1990) 3202–3206.

[2] M.A. Willard, Y. Nakamura, E. David Laughlin, E. Michael McHenry, Magnetic properties of ordered and disordered spinel-phase ferrimagnets, J. Am. Ceram. Soc. 82 (1999) 3342–3346.

[3] M.P. Horvath, Microwave application of soft ferrites, J. Magn. Magn. Mater. 215 (2000) 171–183.

[4] J.D. Adams, L.E. David, G.F. Dionne, E.F. Schloemann, S.N. Stitzer, Ferrite devices and materials, IEEE Trans. Microwave Theory Tech. 50 (2002) 721–737.

[5] Z.H. Zhou, J.M. Xue, J. Wang, $NiFe_2O_4$ nanoparticles formed in situ in silica matrix by mechanical activation, J. Appl. Phys. 91 (2002) 6015–6020.

[6] B.S. Randhawa, Preparation of ferrites from the thermolysis of transition metal ferrioxalate precursors, J. Mater. Chem. 10 (2000) 2847–2852.

[7] B.S. Randhawa, K.J. Sweety, M. Kaur, J.M. Greneche, Synthesis of ferrites, J. Therm. Anal. Calorim. 75 (2004) 101–110.

[8] B.S. Randhawa, M. Kaur, The thermolysis of zinc bis(citrato)ferrate(III) dodecahydrate, J. Radioanal. Nucl. Chem. 256 (2003) 509–511.

[9] A. Vertes, L. Korecz, K. Burger, Mössbauer Spectroscopy, Elsevier, New York, 1979.

[10] B.J. Evans, S.S. Hafner, Mössbauer resonance of Fe^{57} in oxidic spinels containing Cu and Fe, J. Phys. Chem. Solids 29 (1968) 1573–1588.